Journal of the Korean Physical Society, Vol. 75, No. 4, August 2019, pp. 304∼308

Effect of Gd Doping on the Structural and Magnetic Properties of Ni-Cu-Zn-Fe_2O_4

P. Venkata Srinivasa Rao*
Department of Physics, Acharya Nagarjuna University, Guntur, Andhra Pradesh -522510, India and Department of Physics, SS&N College, Narasaraopet, Guntur, Andhra Pradesh - 522601, India

T. Anjaneyulu
Department of Physics, Narasaraopeta Engineering College, Narasaraopeta, Andhra Pradesh - 522601, India

M. Rami Reddy
Department of Physics, Acharya Nagarjuna University, Guntur, Andhra Pradesh - 522510, India

(Received 20 July 2018; revised 8 June 2019; accepted 21 June 2019)

$Ni_{0.5}Cu_{0.25}Zn_{0.25}Gd_xFe_{2-x}O_4$ (x = 0.0, 0.025, 0.05, 0.075, 0.1) ferrites were synthesized using an oxalic-based precursor method. A single phase Ni-Cu-Zn-Gd ferrite was observed from X-ray diffraction (XRD) data except for higher Gd content. For $x = 0.1$, a secondary phase due $GdFe_2O_3$ was observed. The particle size was observed to decrease and the lattice constant to increase with increasing Gd doping concentration. The IR spectra confirmed the existence of bands corresponding to spinel ferrites. The IR band positions were observed to shift towards higher positions with increasing Gd doping concentration. The saturation magnetization, coercivity and remanence magnetization were observed to increase as a result of Gd doping. The substitution of Gd ions in the place of Fe ions resulted in changes in the structural and magnetic properties due to replacement of smaller ionic radii Fe ions by larger ionic radii Gd ions.

PACS numbers: 77.22.−d, 77.22.Gm
Keywords: Ni-Cu-Zn-Gd nanoferrites, Structural properties, Magnetic properties
DOI: 10.3938/jkps.75.304

I. INTRODUCTION

Spinel Ni-Cu-Zn ferrites have potential uses in high frequency applications and in magnetic storage devices [1]. They are used as recording heads, inductors, deflection yokes, transformer cores, *etc.* [2,3]. In recent years, the structural, electrical and magnetic properties of these ferrites with different chemical compositions in different forms, like thin films and nano powder, have been investigated. In these ferrites, partial doping is done in the place of Fe^{3+} ions, and may lead to structural distortion, which can enhance the magnetic properties. Rare-earth doped Ni-Cu-Zn ferrites have improved magnetic and optical properties [4–8]. At higher percentage of rare-earth doping in ferrites usually contributes to the formation of rare-earth secondary phases and is observed for only a few kinds of rare-earth elements [9]. The magnetic properties of the ferrite materials are well known to depend on the type, ionic radius and concentration of the doping ions (magnetic/non-magnetic nature) [10], grain size and morphology of the samples and the methods of preparation [11,12]. Doping these ferrites with various transition elements leads to important changes in their structural, electrical and magnetic properties.

The synthesis of Gd doped Ni-Cu-Zn ferrites is a challenging task because of co-existence of the undesired phase like $GdFeO_3$ along with the spinel. The rare-earth ions are known to play an important role in determining the magnetocrystalline anisotropy in 4f-3d intermetallic compounds [13]. The presence of Gd^{3+} ions influences mainly the magnetic anisotropy of the system. The magnetic properties of ferrites can be changed with the substitution of various kinds of divalent ions or by the introduction of relatively small amount of rare-earth ions. Substitution of rare-earth ions into the spinel structure has been reported to cause structural distortion, strains, and significant modifications of the electrical and magnetic properties [14, 15]. All the rare-earth ions are found to favor the occurrence of secondary phases, resulting in increased bulk density and electrical resistivity [16, 17]. From our literature review, we observed that until now, no researcher has reported on Gd-doped $Ni_{0.5}Cu_{0.25}Zn_{0.25}Fe_2O_4$ ferrite. Therefore, in

*E-mail: pvsrinivasphd@gmail.com

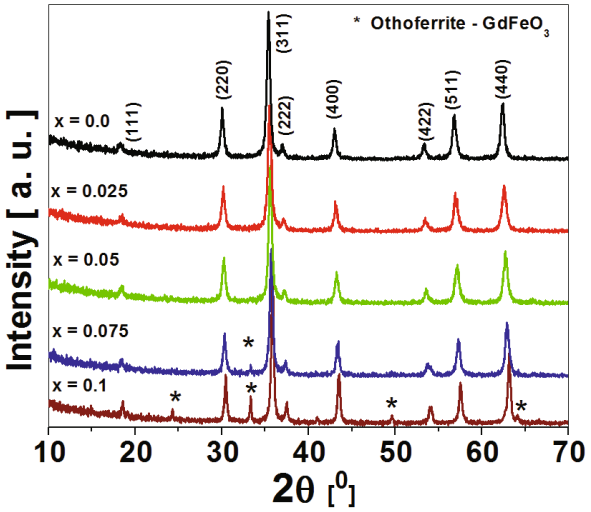

Fig. 1. (Color online) X-ray diffraction patterns of $Ni_{0.5}Cu_{0.25}Zn_{0.25}Gd_xFe_{2-x}O_4$ (x = 0.0, 0.025, 0.05, 0.075, 0.1) ferrites.

this present work, we made an attempt to systematically dope Gd into Ni-Cu-Zn ferrite synthesized using the oxalic-acid based precursor method [18–20] and to investigate structural and magnetic properties on the Gd-doped ferrites. These structural and magnetic properties were examined using X-ray diffraction (XRD), scanning electron microscopy (SEM), Fourier transform infrared spectroscopy (FTIR) and vibrating sample magnetometry (VSM).

II. EXPERIMENTAL PROCEDURE

$Ni_{0.5}Cu_{0.25}Zn_{0.25}Gd_xFe_{2-x}O_4$ (x = 0.0, 0.025, 0.05, 0.075, 0.1) ferrite nanopowders were synthesized using an oxalate-based precursor method [18–20]. All the chemicals used were analytical reagent grade chemicals (Sigma-Aldrich) and had purities $\geq$ 99%. In this synthesis process, nickel nitrate hydrate ($Ni(NO_3)_2{\cdot}6H_2O$), cupric nitrate hydrate ($Cu(NO_3)_2{\cdot}6H_2O$), zinc nitrate hydrate ($Zn(NO_3)_2{\cdot}6H_2O$), gadolinium oxide (Gd_2O_3) and ferric nitrate nonahydrate ($Fe(NO_3)_3{\cdot}9H_2O$) were used as the starting materials. The entire synthesis process is described elsewhere [19]. The resultant mixtures were evaporated on a hot plate at ~150 °C for 2 h. The obtained raw powders were thermally treated at 450 °C for 4 h.

The structural properties of the obtained ferrite powders was measured using Phillips X-ray diffraction (XRD) with a Ni filter and Co Kα radiation (λ = 1.78894 Å). The average grain size (D) was calculated using the most intense peak, the (311) peak, by employing the Scherrer formula. SEM analyses were performed by using a Philips CM-12 scanning electron microscope attached to an energy dispersive X-ray spectrometer (EDS). EDS measurement was carried out to further confirm the composition of the prepared samples. The structural changes with Gd doping in Ni-Cu-Zn ferrites were observed by using an ABB Bomem MB 102 infrared spectrometer equipped with CsI optics and a deuterated triglycine sulfate (DTGS) detector. The samples were mixed with KBr and made in the form of pellets and data were recorded at 4 cm^{-1} resolution (10 consecutive scans were averaged for each spectrum) in the 4000–250 cm^{-1} range. For our study, we have chose the range from 1000–300 cm^{-1}. The room temperature magnetic properties were measured with a vibrating sample magnetometer (VSM 4500).

III. RESULTS AND DISCUSSION

Figure 1 shows the XRD patterns of the $Ni_{0.5}Cu_{0.25}Zn_{0.25}Gd_xFe_{2-x}O_4$ (x = 0.0, 0.025, 0.05, 0.075, 0.1) ferrite samples. The XRD results confirm the presence of a single-phase cubic spinel structure with the space group Fd3m. With higher Gd content x = 0.075 and 0.1, secondary phases corresponding to the Orthoferrite-phase $GdFeO_3$ were observed. These secondary phases might be due to unreacted Gd ions at higher doping concentrations [15]. With higher Gd content in the samples, the dilution of the rare-earth elements will not take place properly. Therefore, if the rare-earth doping concentration is higher than a certain limit for a particular element, secondary peaks will be observed in the samples.

The grain size D was calculated using the most intense (311) peak of the XRD patterns and Scherrer's formula. The grains were observed to decrease in size with increasing Gd doping concentration, as shown in Table 1. Furthermore, the energy bond for Gd^{3+}-O^{2-} is higher than that for Fe^{3+}-O^{2-} [3]. Therefore the doping of Gd^{3+} ions in Ni-Cu-Zn ferrites produces internal lattice stress, which will hinder the grain growth [21]. The lattice constant was observed to increase slightly with increasing Gd doping concentration, as shown in Table 1. The increase in the lattice constant is due to replacement of smaller ionic radii Fe^{3+} ions (0.69 Å) with higher ionic radii Gd^{3+} ions (0.938 Å) [15,22]. The ionic radii of Gd^{3+} ions are large enough for octahedral [B] sites. Even with a small doping of Gd^{3+} ions in place of Fe^{3+} ions, they will enter into the octahedral sites by rearranging the cations between the octahedral and the tetrahedral sites in order to minimize the free energy of the system. A partial migration of Fe^{3+} ions from octahedral to tetrahedral sites due to Gd^{3+} ions substitution may be accompanied by the opposite transfer with an equivalent number of Fe^{3+} ions from tetrahedral to octahedral sites in order to relax the strain at the octahedral sites [23]. Also, the larger Gd ions will cause diffusion at the grain boundaries in the spinel ferrites even with a small number of Gd ions, which will result in the precipitation of more of the crystalline or the amorphous-like orthoferrite phase

Table 1. Grain size (D), lattice constant (a), X-ray density (d_{XRD}), IR frequencies ν_1 and ν_2, saturation magnetization (M_S), coercivity (H_c) and remanence magnetization (M_r) of $Ni_{0.5}Cu_{0.25}Zn_{0.25}Gd_xFe_{2-x}O_4$ (x = 0.0, 0.025, 0.05, 0.075, 0.1) ferrites.

x	D (nm)	a (Å)	d_{XRD}	ν_1 (cm^{-1})	ν_2 (cm^{-1})	M_S (emu/g)	H_C (Oe)	M_R (emu/g)
0.0	27	8.421	5.269	406	569	38.6	202	11.8
0.025	23	8.432	5.325	411	571	41.2	121	17.8
0.05	21	8.451	5.382	413	572	42.3	323	19.4
0.075	18	8.477	5.438	418	573	45.8	778	28.5
0.10	17	8.498	5.495	421	576	515	981	26.3

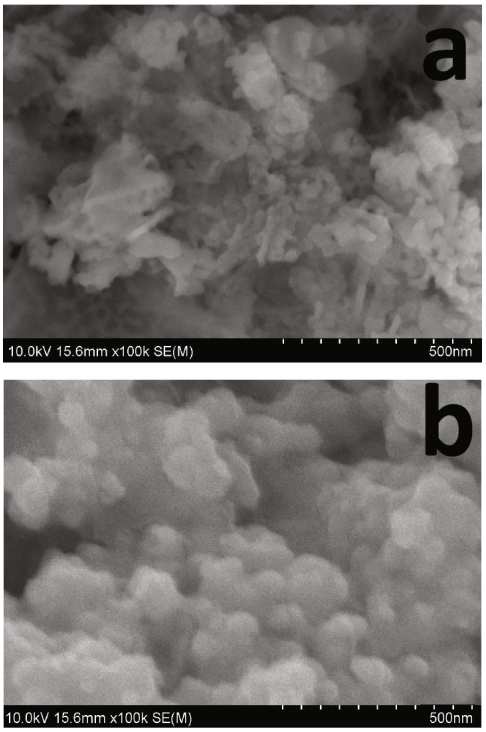

Fig. 2. SEM images of $Ni_{0.5}Cu_{0.25}Zn_{0.25}$ $Gd_xFe_{2-x}O_4$ ((a) x = 0.0 and (b) x = 0.1) ferrites.

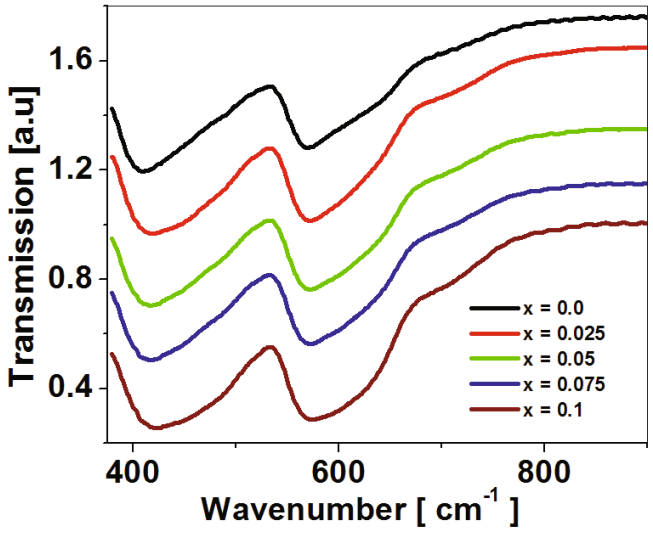

Fig. 3. (Color online) FTIR spectra of $Ni_{0.5}Cu_{0.25}Zn_{0.25}$ $Gd_xFe_{2-x}O_4$ (x = 0.0, 0.025, 0.05, 0.075, 0.1) ferrites.

($RFeO_3$) in the samples [24]. Therefore, the variation in the lattice constant indicates the partial substitution of Gd^{3+} ions in place of Fe^{3+} ions.

The X-ray density for $Ni_{0.5}Cu_{0.25}Zn_{0.25}Gd_xFe_{2-x}O_4$ (x = 0.0, 0.025, 0.05, 0.075, 0.1) samples was calculated from the molecular weight and the volumes of the unit cell by using the

$$d_x = \frac{8M}{Na^3}[\mathrm{g/cm^3}], \quad (1)$$

where M is molecular weight, N is Avogadro's number and a is lattice parameter. The X-ray densities for various Gd doping concentrations are given in Table 1, where the X-ray density can be seen to increase with increasing Gd doping concentration.

SEM micrographs of pure and Gd doped Ni-Cu-Zn-Gd ferrite powder are shown in Figs. 2(a) and (b). The micrographs show nanosize grains in the synthesized samples and a slight agglomeration in the samples as a result of the nano nature. With increased Gd doping, a slight change in the grain size and texture can be observed.

The formation of the ferrite phase is further supported by the IR data. IR spectra for $Ni_{0.5}Cu_{0.25}Zn_{0.25}$ $Gd_xFe_{2-x}O_4$ (x = 0.0, 0.025, 0.05, 0.075, 0.1) samples were recorded in the range 300–1000 cm^{-1}, and the results are shown in Fig. 3 with the corresponding values given in Table 1. No absorption bands were observed above 1000 cm^{-1}. The IR spectra showed two main absorption bands, ν_1 and ν_2 as a common feature for all the ferrites samples [25,26]. The band ν_1 (near 400 cm^{-1}) is due to octahedral complexes (metal-oxygen vibration in octahedral sites), and the band ν_2 (near 600 cm^{-1}) arises due to tetrahedral complexes (the stretching vibration of the tetrahedral metal-oxygen bond). The difference in the positions of the two strong bands ν_1 and ν_2 could be related to the difference in the Fe^{3+}-O^{2-} distances for the A-sites and the B-sites. The presence of band ν_1 at 450 cm^{-1} is the evidence for the presence Gd ions instead

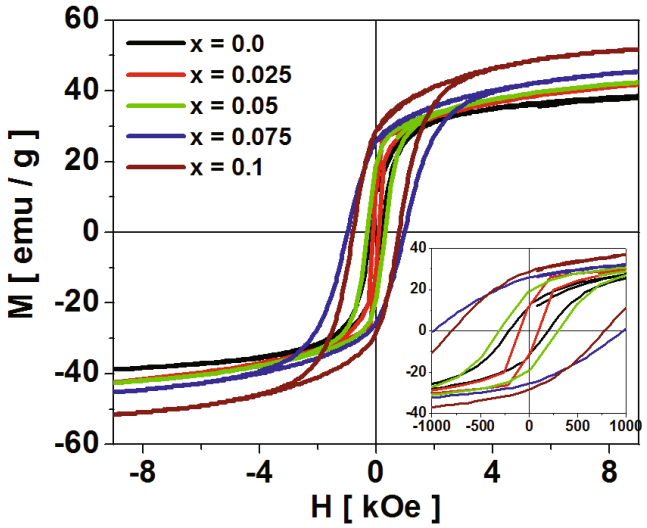

Fig. 4. (Color online) M-H curves of $Ni_{0.5}Cu_{0.25}Zn_{0.25}Gd_xFe_{2-x}O_4$ (x = 0.0, 0.025, 0.05, 0.075, 0.1) ferrites. The inset shows the expanded lower field curves.

of Fe in B sites, and the ν_1 bands are due to stretching vibrations of (Gd^{3+}-O^{2-}) [22]. The band positions were observed to shift towards higher wave number with increasing Gd doping concentration. This change may be attributed to the change in the grain size due to Gd doping concentration.

The magnetization curves for $Ni_{0.5}Cu_{0.25}Zn_{0.25}Gd_xFe_{2-x}O_4$ (x = 0.0, 0.025, 0.05, 0.075, 0.1) samples measured at room temperature are show in Fig. 4. The parameters derived from the magnetization curves are presented in Table 1. All the samples exhibited the ferromagnetic behavior, and the M-H curve show a soft magnetic behavior. Therefore, such samples may find applications in high-frequency devices. The M-H curves, show that, with increasing Gd concentration, the saturation magnetization, coercivity and remanence magnetization increased significantly. The decrease in coercivity at a Gd content of 0.025 in our samples may be due to several reasons, such as a change in the defect structure as a result of doping. Generally, the coercivity is very well known to increase with increasing single-domain grain size. However, when the grain size increases or attains a multidomain nature, then the coercivity starts to decrease [27]. Similar behavior was observed previously for other kinds of ferrites [28, 29]. The increase in the coercivity of the samples with Gd > 0.025 doping is due to the appearance of the orthoferrite phase at higher Gd doping concentration. The orthoferrites, which co-exist with the ferrites phase in the samples, will try to impedes the motion of ferrite grains, resulting in enhanced coercivity. The saturation magnetization in nanoparticles can be estimated from the magnetic moments of Fe^{3+} ions at the tetrahedral (A) and the octahedral (B) sites, respectively. The difference in the magnetization values is mainly due to the difference in the Fe^{3+} cation distribution between these two sites [30,31]. The Gd^{3+} ions have 7 μB and the Fe^{3+} ions have 5 μB. Due to the large difference between the Gd^{3+} and the Fe^{3+} ions, the higher magnetic moment of the Gd^{3+} ions dominates the smaller magnetic moment of Fe^{3+} ions. Therefore, the magnetization was enhanced with increasing number of Gd^{3+} ions in all the samples. Therefore, the Gd doping in Ni-Cu-Zn ferrites had significant effects on the magnetic properties of these ferrites.

IV. CONCLUSIONS

$Ni_{0.5}Cu_{0.25}Zn_{0.25}Gd_xFe_{2-x}O_4$ (x = 0.0, 0.025, 0.05, 0.075, 0.1) ferrite nano powders were successfully synthesized using the oxalate-based precursor method. XRD spectra showed a single-phase cubic spinel structure. The grain size increased with increasing Gd content, and the lattice constant increased slightly. The IR spectra confirmed that the ferrite phase was sensitive to Gd doping. The saturation magnetization, coercivity and remanence magnetization increased with increasing Gd concentration.

ACKNOWLEDGMENTS

The authors thank the Sophisticated Analytical Instrumentation Facility (SAIF), Indian Institute of Technology (IIT) Madras, for measurements. P. V. Srinivasa Rao thanks University Grants Commission (UGC), government of India, for granting a scholarship under the Faculty Development Program (FDP).

REFERENCES

[1] C. M. Dimri, C. S. Kashyap and D. C. Dube, Phys. Status Solidi A **207**, 396 (2010).
[2] T. Nakamura, J. Magn. Magn. Mater. **168**, 285 (1997).
[3] H. Harzali *et al.*, J. Magn. Magn. Mater. **419**, 50 (2016).
[4] M. M. Eltabey, K. M. El-Shokrofy and S. A. Gharbia, J. Alloys Compd. **509**, 2473 (2011).
[5] M. Kaiser, J. Alloys Compd. **719**, 446 (2017).
[6] M. H. Abdellatif, G. M. El-Komy and A. A. Azab, J. Magn. Magn. Mater. **442**, 445 (2017).
[7] R. Hochschild and H. Fuess, J. Mater. Chem. **10**, 539 (2000).
[8] L. Yang *et al.*, J. Mater. Sci.: Mater. Electron. **26**, 6848 (2015).
[9] P. K. Roy and J. Bera, J. Magn. Magn. Mater. **321**, 247 (2009).
[10] Y. He *et al.*, Sci. Adv. Mater. **7**, 1809 (2015).
[11] S. Suguna, S. Shankar, S. K. Jaganathan and A. Manikandan, J. Supercond. Nov. Magn. **30**, 691 (2017).
[12] G. Padmapriya *et al.*, J. Supercond. Nov. Magn. **29**, 2141 (2016).

[13] L. Zhao *et al.*, J. Magn. Magn. Mater. **309**, 11 (2007).
[14] K. K. Bharathi, J. A. Chelvane and G. Markandeyulu. J. Magn. Magn. Mater. **31**, 3677 (2009).
[15] K. K. Bharathi *et al.*, Phys. Rev. B **77**, 172401 (2008).
[16] O. M. Hemeda, M. Z. Said and M. M. Barakat, J. Magn. Magn. Mater. **224**, 132 (2001).
[17] A. R. Buenoa, M. L. Gregori and M. C. S. N'obrega, Mater. Chem. Phys. **105**, 229 (2007).
[18] A. T. Raghavender, S. E. Shirsath and K. V. Kumar, J. Alloys Compd. **509**, 7004 (2011).
[19] D. G. Wickham, Inorg. Synth. **9**, 152 (1967).
[20] N. D. Chaudhari *et al.*, Mater. Res. Bull. **45**, 1713 (2010).
[21] M. T. Farid *et al.*, J. Magn. Magn. Mater. **422**, 337 (2017).
[22] H. Harzali *et al.*, J. Magn. Magn. Mater. **460**, 89 (2018).
[23] L. Kumar and M. Kar, Ceram. Int. **38**, 4771 (2012).
[24] M. Yehia, S. M. Ismail and A. Hashhash, J. Supercond. Nov. Magn. **27**, 771 (2014).
[25] S. Hafner, Z. Kristallogr. **115**, 331 (1961).
[26] R. D. Waldron, Phys. Rev. **99**, 1727 (1955).
[27] M. Desai *et al.*, J. Magn. Magn. Mater. **231**, 108 (2001).
[28] M. Desai *et al.*, J. Appl. Phys. **91**, 7592 (2002).
[29] J. Dash *et al.*, J. Magn. Soc. Jpn. **22**, 176 (1998).
[30] Y. Q. Jia, J. Solid State Chem. **95**, 184 (1991).
[31] A. Manikandan, L. J. Kennedy, M. Bououdina and J. J. Vijava, J. Magn. Magn. Mater. **349**, 249 (2014).